Article

Synergistic Anion–$(\pi)_n$–π Catalysis on π-Stacked Foldamers

BORNHOF, Anna-Bea, *et al*.

Abstract

In this report, we demonstrate that synergistic effects between π–π stacking and anion−π interactions in π-stacked foldamers provide access to unprecedented catalytic activity. To elaborate on anion–(π)n–π catalysis, we have designed, synthesized and evaluated a series of novel covalent oligomers with up to four face-to-face stacked naphthalenediimides (NDIs). NMR analysis including DOSY confirms folding into π stacks, cyclic voltammetry, steady-state and transient absorption spectroscopy the electronic communication within the π stacks. Catalytic activity, assessed by chemoselective catalysis of the intrinsically disfavored but biologically relevant addition reaction of malonate half thioesters to enolate acceptors, increases linearly with the length of the stacks to reach values that are otherwise beyond reach. This linear increase violates the sublinear power laws of oligomer chemistry. The comparison of catalytic activity with ratiometric changes in absorption and decreasing energy of the LUMO thus results in superlinearity, that is synergistic amplification of anion−π catalysis by remote control [...]

Reference

BORNHOF, Anna-Bea, *et al*. Synergistic Anion–$(\pi)_n$–π Catalysis on π-Stacked Foldamers. *Journal of the American Chemical Society*, 2018, vol. 140, no. 14, p. 4884-4892

DOI : 10.1021/jacs.8b00809

JACS
JOURNAL OF THE AMERICAN CHEMICAL SOCIETY
Article
Cite This: J. Am. Chem. Soc. 2018, 140, 4884−4892
pubs.acs.org/JACS

Synergistic Anion−$(\pi)_n$−π Catalysis on π-Stacked Foldamers

Anna-Bea Bornhof,[†] Antonio Bauzá,[‡] Alexander Aster,[§] Marion Pupier,[†] Antonio Frontera,[‡] Eric Vauthey,[§] Naomi Sakai,[†] and Stefan Matile*[,†]

[†]Department of Organic Chemistry, [§]Department of Physical Chemistry, University of Geneva, CH-1211 Geneva, Switzerland
[‡]Department de Química, Universitat de les Illes Balears, Carretera de Valldemossa km 7.5, 07122 Palma de Mallorca, Baleares, Spain

Supporting Information

ABSTRACT: In this report, we demonstrate that synergistic effects between π−π stacking and anion−π interactions in π-stacked foldamers provide access to unprecedented catalytic activity. To elaborate on anion−$(\pi)_n$−π catalysis, we have designed, synthesized and evaluated a series of novel covalent oligomers with up to four face-to-face stacked naphthalenediimides (NDIs). NMR analysis including DOSY confirms folding into π stacks, cyclic voltammetry, steady-state and transient absorption spectroscopy the electronic communication within the π stacks. Catalytic activity, assessed by chemoselective catalysis of the intrinsically disfavored but biologically relevant addition reaction of malonate half thioesters to enolate acceptors, increases linearly with the length of the stacks to reach values that are otherwise beyond reach. This linear increase violates the sublinear power laws of oligomer chemistry. The comparison of catalytic activity with ratiometric changes in absorption and decreasing energy of the LUMO thus results in superlinearity, that is synergistic amplification of anion−π catalysis by remote control over the entire stack. In computational models, increasing length of the π-stacked foldamers correlates sublinearly with changes in surface potentials, chloride binding energies, and the distances between chloride and π surface and within the π stack. Computational evidence is presented that the selective acceleration of disfavored but relevant enolate chemistry by anion−π catalysis indeed originates from the discrimination of planar and bent tautomers with delocalized and localized charges, respectively, on π-acidic surfaces. Computed binding energies of keto and enol intermediates of the addition reaction as well as their difference increase with increasing length of the π stack and thus reflect experimental trends correctly. These results demonstrate that anion−$(\pi)_n$−π interactions exist and matter, ready for use as a unique new tool in catalysis and beyond.

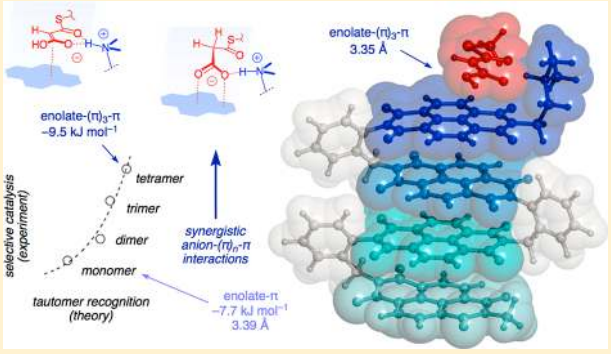

INTRODUCTION

Common aromatic compounds have electron clouds above and beneath their surfaces. The result are negative quadrupole moments perpendicular to the π plane ($Q_{ZZ} < 0$) that naturally attract cations rather than anions.[1] If these compounds are, however, substituted with strong electron withdrawing groups, the quadrupole moment can be inverted, thus making them π acidic. Anion binding to such π acids has been confirmed to occur in solid and solution state with functional relevance in self-assembly and transport.[2] Evolving from the ground state to anion stabilization in the transition state, anion−π catalysis has been introduced recently.[3] Using electric fields, we have demonstrated the importance of polarizability in anion−π catalysis.[4] In a complementary approach, large and highly polarizable fullerene surfaces supported by induced aromatic dipoles rather than inverted quadrupole moments have been found to provide access to anion−π interactions of highest functional relevance.[5] Toward polarizing the π-acidic surfaces by charge delocalization over systems as large as possible, we here introduce synergistic anion−$(\pi)_n$−π interactions in π-stacked foldamers. Theoretical studies have predicted early on that synergistic anion−$(\pi)_n$−π interactions would provide access to exceptionally strong anion−π interactions already on simple, uniform or mixed π dimers of benzene and hexafluorobenzene, i.e., minimalist aromatics that essentially fail to interact with ions as monomers.[6]

Naphthalenediimides (NDIs)[7] have emerged as particularly attractive framework to elaborate on anion−π interactions because their intrinsic quadrupole moment is highly positive and can be easily varied with core substituents.[8] These properties have been essential in constructing and proving functional anion−π transporters and catalysts.[3,4,8] A variety of materials based on NDI stacks has been developed over the past decades[7,9−23] for organoelectronics,[7,9] synthetic ion channels,[8,10] sensors and catalysts.[11] Most of these materials are based on noncovalent assemblies of NDIs that form structural motifs like helices,[12] nanotubes,[13,14] sheets[15] or spheres.[16] For a better understanding of these large assemblies, efforts have been made to synthesize covalent, well-defined

Received: January 22, 2018
Published: April 2, 2018

DOI: 10.1021/jacs.8b00809
J. Am. Chem. Soc. 2018, 140, 4884−4892

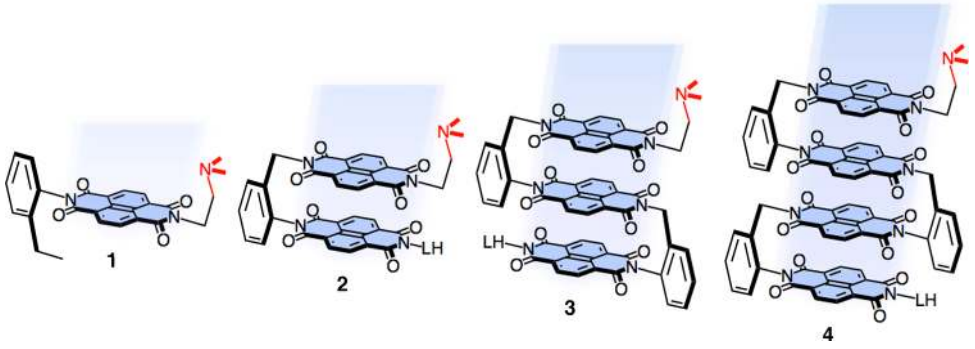

Figure 1. Structure of NDI foldamers **1**–**4** made to elaborate on synergistic anion–$(\pi)_n$–π catalysis.

structures, and electronic communication as well as spectroscopic behavior have been investigated.[17,18] However, contrary to extensive studies on donor–acceptor foldamers with NDIs and π-basic partners,[19] most of these covalent NDI oligomers are limited to two units. Larger discrete stacks were synthesized by self-assembly on DNA[20] and rigid-rod templates,[10] dendrimers,[21] or polyrotaxane chemistry.[22]

Herein we report the design, synthesis and evaluation of discrete, monodisperse NDI stacks containing up to four covalently connected, face-to-face stacked NDIs. By experimental and computational studies on their folding behavior, electronic communication and catalytic activities, we aim to demonstrate the existence and relevance of synergistic anion–$(\pi)_n$–π catalysis.

RESULTS AND DISCUSSION

The NDI monomer **1**, dimer **2**, trimer **3** and tetramer **4** were synthesized in a linear manner (Figure 1). Starting from dianhydride **5**, NDI formation with amines **6** and **7** afforded monomer **1** in a single step (Scheme 1). The side products with two identical imide substituents were removed by column chromatography. Oligomer synthesis was initiated from the same dianhydride **5**. The Boc-protected benzyl turn **8** and the leucyl-hexyl (LH) tail **9** were introduced in a basic condensation reaction yielding the monomeric building block **10**. The byproduct **11** with two LH tails was isolated for use as negative control in anion–$(\pi)_n$–π catalysis. Deprotection of NDI **10**, reaction with another NDA **5** and condensation with the dimethylamine headgroup **7** gave the desired NDI dimer **2**. The dimeric building block **12** was prepared similarly from the same monomeric building block **10** using turn **8** instead of tertiary amine **7** in the condensation reaction. This dimeric building block **12** could be further converted to either trimer **3** or trimeric building block **13** using the same protocols as for dimer **2** or dimeric building block **12**, respectively. Finally, tetramer **4** was prepared from trimeric building block **13** by deprotection of the of the amine and successive condensation with one equivalent of NDA **5** and the catalytic headgroup **7**.

Foldamer[24] Characterization. In the ^{1}H NMR spectrum of monomer **1**, the NDI protons appeared as a single peak at 8.8 ppm (Figure 2A). This deshielded resonance nicely illustrated the electron-deficient nature of the aromatic system. In dimer **2**, the NDI signals split into six resolved doublets, all with nearly identical coupling constants and spread out toward 8.0 ppm. This variable upfield shift was in agreement with the folding of dimer **2** into a face-to-face stack, with NDI protons exposed to the ring current from the proximal second NDI. Different shifts for six out of eight possible doublets suggested

Scheme 1. Foldamer Synthesis[a]

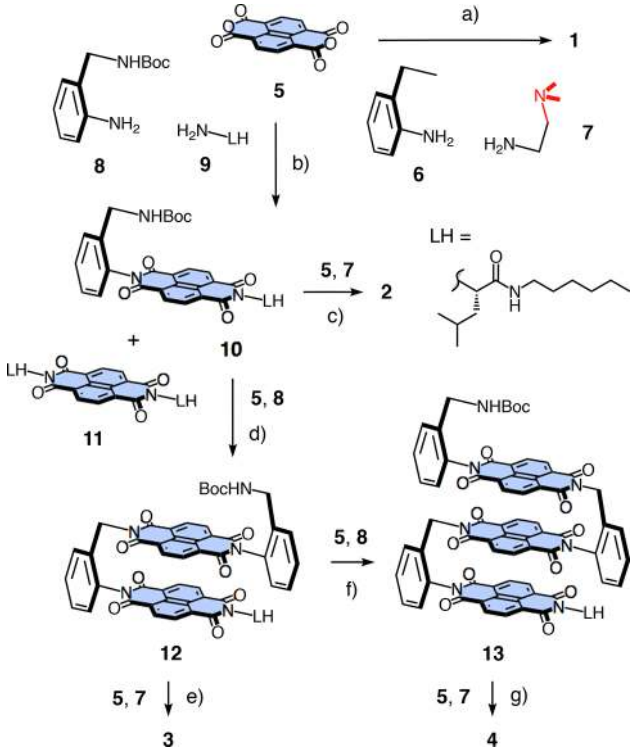

[a](a) 1. **6**, AcOH, 120 °C, 1.5 h, 2. **7**, AcOH, 120 °C, 5 h, 20%; (b) 1. **8**, TEA, toluene/DMF 2:1, 120 °C, Ar, 30 min, 2. **9**, AcOH, toluene/DMF 2:1, 120 °C, Ar, 1 h, 30% (**10**), 5% (**11**); (c) 1. TFA/CH_2Cl_2 1:1, rt, 1 h, 2. **5**, TEA, toluene/DMF 2:1, 120 °C, Ar, 1.5 h, 3. **7**, TEA, toluene/DMF 2:1, 120 °C, Ar, 30 min, 44%; (d) 1. TFA/CH_2Cl_2 1:1, rt, 1 h, 2. **5**, TEA, toluene/DMF 2:1, 120 °C, Ar, 1.5 h, 3. **8**, AcOH, toluene/DMF 2:1, 120 °C, Ar, 4 h, 55%; (e) 1. TFA/CH_2Cl_2 1:1, rt, 1 h, 2. **5**, TEA, toluene/DMF 2:1, 120 °C, Ar, 2.5 h, 3. **7**, toluene/DMF 2:1, 120 °C, Ar, 1 h, 57%; (f) 1. TFA/CH_2Cl_2 1:1, rt, 1 h, 2. **5**, TEA, toluene/DMF 2:1, 120 °C, Ar, 2.5 h, 3. **8**, AcOH, toluene/DMF 2:1, 120 °C, Ar, 3 h, 41%; (g) 1. TFA/CH_2Cl_2 1:1, rt, 1 h, 2. **5**, TEA, toluene/DMF 2:1, 120 °C, Ar, 1 h, 3. **7**, toluene/DMF 2:1, 120 °C, Ar, 30 min, 30%.

that the environment of all but two NDI protons differs (Figures 2A, S33–S39). This nearly maximal peak separation confirmed expectations from computational simulations that in dimer **2**, the long axes of two cofacial NDI planes are twisted out of colinearity (29.8°, Figure S14, see below).

With trimer **3** and tetramer **4**, more doublets appeared upfield, consistent with the new NDIs being sandwiched between two neighbors in the π-stacked foldamers. This trend

DOI: 10.1021/jacs.8b00809
J. Am. Chem. Soc. 2018, 140, 4884–4892

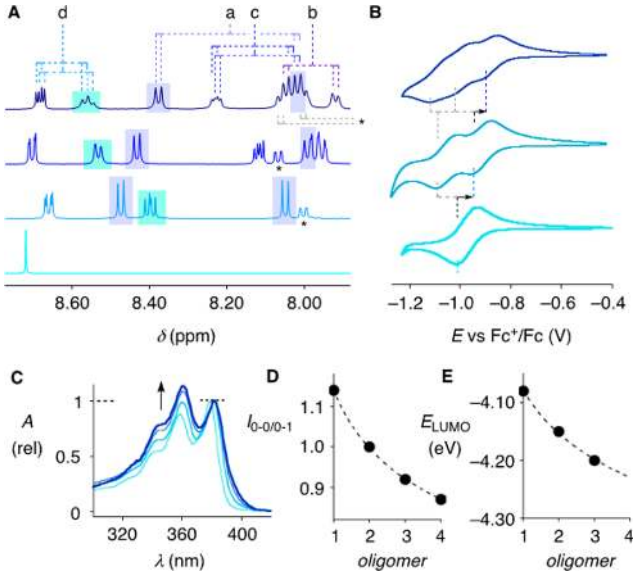

Figure 2. (A) Diagnostic region of ^{1}H NMR spectra of monomer **1**, dimer **2**, trimer **3** and tetramer **4** (bottom to top) in THF-d_8/$CDCl_3$ 3:1, with assignments to NDIs a (amine terminus), b, c and d (LH terminus) for **4** (*, signals from benzyl turns). (B) Cyclic voltammograms (CVs) of NDIs **1**, **2** and **3** (bottom to top) in MeCN with a glassy carbon working electrode, a calomel reference electrode, $TBAPF_6$ (0.1 M) as supporting electrolyte and a scan rate of 50 mV s^{-1}. (C) Normalized UV−vis absorption spectra of **1**, **2**, **3** and **4** in THF (light to dark blue). (D) Dependence of absorbance ratio on oligomer length, i.e., monomer per oligomer, with power fit; from panel C. (E) Dependence of LUMO energies on oligomer length, with power fit; from panel B.

was as expected for folding into ordered, face-to-face π-stacked oligomers. For all foldamers, a tentative assignment of up to four separated doublets to each individual NDI in the stacks was possible by COSY, HMBC and HSQC 2D NMR spectroscopy (Figures 2A, S33−S58). High-resolution 2D spectra from computer-assisted aliasing techniques, developed in-house,[25] were needed to resolve the fine-structured signal clusters (rather than broad peaks) that are characteristic for oligomers in ordered (rather than disordered) conformation. Additional signals for NDI protons were not observed. This presence of only one set of signals in all spectra, in $CDCl_3$ and THF-d_8/$CDCl_3$ 3:1 (see catalysis), demonstrated that, independent of stack length, conformers other than the robust π-stacked foldamers are at most a mere minority (Figure 2A). Very strong preference for a π-stacked conformation was further demonstrated by the independence on solvent and temperature up to 100 °C in competing toluene in UV−vis absorption studies (*vide infra*).[24,26]

In the DOSY 2D NMR spectra, a diffusion coefficient of D = 4.22 × 10^{-10} m^2 s^{-1} was measured for trimer **3** (Figure S28). According to Stokes−Einstein equation assuming a spherical molecule, this corresponded to a radius of 9.65 Å.[27] The geometry-optimized structure of trimer **3** showed a spherical radius of 9.9 Å in good agreement with the experimental value (Figure S27, see below). The same experiment was performed for tetramer **4**. In $CDCl_3$ at 298 K, a diffusion coefficient of 3.98 × 10^{-10} m^2 s^{-1} was extracted from the DOSY spectra (Figure S28). The slower diffusion of the larger tetramer **4** compared to trimer **3** was as expected. The resulting spherical radius of 10.23 Å was again close to the theoretical value of 10.8 Å of the geometry-optimized structure (Figure S27).

Cyclic voltammetry (CV) and differential pulse voltammetry measurements (DPV) were performed in MeCN with a 0.1 M solution of $TBAPF_6$ (Figures 2B, S6). Monomer **1** exhibited a one-electron reduction wave at V = −1.02 V corresponding to the formation of the radical anion $NDI^{\bullet-}$ (Figure 2B, bottom). With dimer **2** and trimer **3**, this first reduction wave split into the separated respective reduction waves for each NDI. The maximum of the first wave shifted to more positive potentials with increasing foldamer length, from V = −1.02 V for monomer **1** to V = −0.95 V for dimer **2** and V = −0.90 V for trimer **3** (Figure 2B). These shifts of up to 120 mV calculated to a decrease of the LUMO energy from −4.08 eV to −4.20 eV against −5.10 eV for Fc^+/Fc (Table 1). As for the similar results obtained with mechanically bonded discrete NDI stacks,[22] we interpreted this lowering of the LUMO level to be caused by favorable electronic communication between the NDIs in the stacks.

Identical trends were observed in THF/CH_2Cl_2 3:1 (almost the solvent mixture used for catalysis, see below), but the individual maxima were not resolved (Figure S7). The poor resolution with trimer **3** also in MeCN (Figure 2B) and

Table 1. Characteristics of Anion−$(\pi)_n$−π Catalysts[a]

oligo[b]	$I_{0\text{-}0/0\text{-}1}$[c]	E_{LUMO}[d] (eV)	$d_{\pi-\pi}$[e]	MEP[f] (kJ mol^{-1})	E_{int}[g] (Cl)	$d_{Cl\text{-}\pi}$[h]	E_{int}[i] (Cl)	$d_{e\text{-}\pi}$[j]	E_{int}[k] (enol)	$d_{k\text{-}\pi}$[l]	E_{int}[m] (keto)	ΔE_{int}[n]	A/D[o]
1	1.14	−4.08	–	100.0	−0.1	3.10	−133.7	3.39	−183.9	2.91	−176.2	7.7	1.8
2	1.00	−4.15	3.53	123.5	−3.3	3.09	−137.5	3.37	−186.0	2.88	−178.1	8.7	2.8
3	0.92	−4.20	3.48	125.1	−5.8	3.08	−140.0	3.36	−187.3	2.70	−178.3	9.0	7.2
4	0.87	nd	3.46	127.6	−8.3	3.07	−141.7	3.35	−188.5	2.69	−179.0	9.5	10.4
hyp	–	–	3.44	129.0	−12.1	3.07	−142.7	–	–	–	–	–	–

[a]Distances d in Å, energies E in kJ mol^{-1}. [b]Oligomers, see Figure 1. hyp: Hypothetical pentamer. **1′−4′**: Hypothetical oligomers with one methyl terminus and one correct amine terminus **1″−4″**: Hypothetical oligomers with two methyl termini, see Figure 5. [c]Absorbance of the 0-0 divided by the absorbance of the 0-1 vibronic transition, Figure 2C. [d]Energy of the LUMO in eV against vacuum, assuming −5.10 eV for Fc^+/Fc. [e−n]Computational data. [e]Distance between the first two π planes, Figure S13. [f]Maximal molecular electrostatic potential on the external π surface, Figure S15. [g]Interaction energy between the chloride anions and the external π surface of **1″−4″** (without covalent counterion), Figure 5. [h]Distance between Cl^- and **1′−4′** (with covalent counterion), Figure 5. [i]Interaction energy between Cl^- and **1′−4′**, Figure 5. [j]Distance between the enol tautomer of conjugate base of **14′** (Me instead of PMP thioester) and **1′−4′**, Figure 6. [k]Interaction energy between enol tautomer of **14′** and **1′−4′**, Figure 6. [l]Distance between the keto tautomer of **14′** and **1′−4′**, Figure 6. [m]Interaction energy between the keto tautomer of **14′** and **1′−4′**, Figure 6. [n]Difference in interaction energy of enol and keto tautomers with **1′−4′**. [o]Yield of addition (**16**)/yield of decarboxylation (**17**). Reactions were conducted with 200 mM **14**, 20 mol % catalysts **1−4** and 2 M acceptor **15** at 20 °C in THF-d_8/$CDCl_3$ 3:1, and monitored by ^{1}H NMR spectroscopy. Total conversion (A + D) was always almost quantitative (>90%), reproducibility within 3.6% for nine independent experiments (Figure 7).

DOI: 10.1021/jacs.8b00809
J. Am. Chem. Soc. 2018, 140, 4884−4892

limitations with regard to solubility suggested that measurements with tetramer **4** are meaningless.

The UV−vis absorption spectra of foldamers **1**−**4** in THF exhibited the two main maxima below 400 nm that can be assigned to the 0-0 and 0-1 vibronic transitions (Figure 2C).[28] For monomer **1**, the absorbance of the first 0-0 band at 381 nm was stronger, the absorbance ratio of the two maxima was $I_{0\text{-}0/0\text{-}1}$ = 1.14 (Table 1). With increasing length of the foldamer, this ratio inverted to $I_{0\text{-}0/0\text{-}1}$ = 0.87 for tetramer **4** (Figure 2C, Table 1). The dependence of $I_{0\text{-}0/0\text{-}1}$ on the number of monomers per foldamer was sublinear and in good agreement with a power fit (Figure 2D). The sublinear power dependence, characteristic for diminishing returns with increasing oligomer length, applied also to the decrease in LUMO energies, although the availability of only three data points naturally limited significance (Figure 2E).

The ratiometric change of the 0-0 and 0-1 vibronic bands has been shown to be a good measure for the electronic coupling within π stacks.[29] An inversion of absorbance ratio has been assigned regularly to $\pi-\pi$ stacking in noncovalent self-assemblies of NDIs.[13,14,18] Moreover, the same phenomenon has been observed in covalent perylenediimide stacks, thus supporting the presence of extensive electron sharing between the NDI monomers in the here introduced series of foldamers.[29,30]

Inversion of ratiometric absorption with sublinear dependence on stack length was observed in all solvents tested, including $CHCl_3$, THF, MeCN and toluene (Figure S8). The ratiometric absorption of trimer **3** in toluene did not change with increasing temperatures up to 100 °C (Figure S10). This insensitivity toward different solvents and the resistance toward thermal denaturation in a most competitive solvent suggested that the π-stacked NDI foldamers are very stable.

Transient absorption spectra upon excitation at 385 nm were recorded for the monomeric building block **10** and trimeric building block **13** (Figures 3, S11). After excitation of

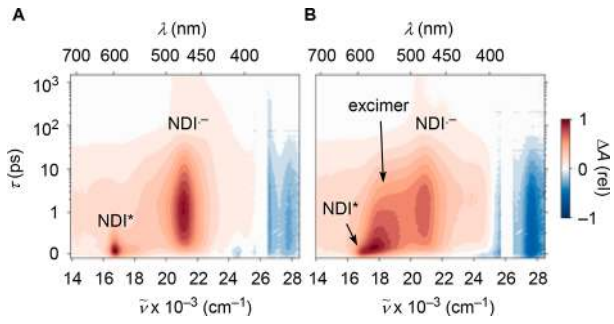

Figure 3. Transient absorption spectra of monomeric building block **10** (A) and trimeric building block **13** (B) in acetonitrile upon excitation at 385 nm.

monomer **10**, a fast decrease of the excited state absorption band at 597 nm and the stimulated emission at 407 nm with a parallel rise of the NDI radical anion band at 475 nm was consistent with photoinduced electron transfer from the benzyl turn to the NDI (Figure 3A).[31,32] In agreement with charge recombination, the $NDI^{\bullet-}$ band subsequently decayed simultaneously with the ground state bleach. Note that the rise of the excited state absorption from −0.1 to +0.1 ps originated from the finite time resolution of the setup, which is about 200 fs. The occurrence of the $NDI^{\bullet-}$ band at this early time steps showed that the electron transfer rate is on the order of the instrument response function. In trimer **13**, the interaction of the stacked NDI units led to a blue shift of the excited state absorption to a broad maximum around 560 nm, indicating a delocalization of the excitation to an excimer-like state (Figure 3B). This excimer state then decayed to the $NDI^{\bullet-}$. Compared to monomer **10**, this radical anion band was spectrally broadened. As with the broadening of the CV reduction waves in longer foldamers (Figure 2B), this finding supported a delocalization of the anion over the stacked NDIs in trimer **13**. A detailed description of the ultrafast photochemistry of π-stacked NDI foldamers will follow in an upcoming publication.

Without substituents in their core, NDIs are essentially not fluorescent because intersystem crossing from the first singlet excited state to the triplet manifold is very fast (<200 fs).[32] With monomer **10**, electron transfer from the benzyl turn to the NDI (Figure 3A) further weakened emission intensity (Figure S12). With dimer **12** and trimer **13**, excimer formation (Figure 3B) resulted in excimer emission, which was also very weak but clearly detectable in steady-state experiments (Figure S12).

Computational Studies. Theoretical calculations on the BP86-D3/def2-TZVP level with dispersion correction in THF continuum[5] were initiated with simplified model oligomers **2″**−**4″** with two methyl termini. Face-to-face π-stacked foldamers were identified as most stable conformers independent of oligomer length (Figures 4A, S25, S26). Completely unfolded

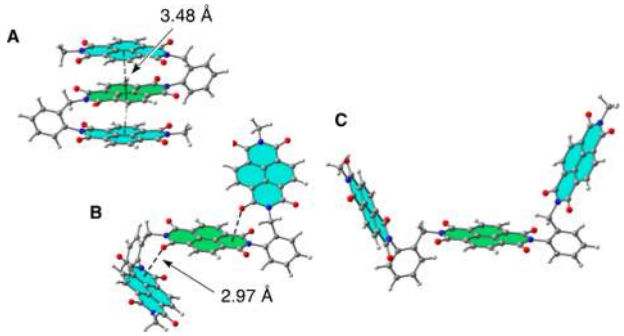

Figure 4. Conformational analysis of trimer **3″** (Me termini) covering (A) face-to-face π-stacked foldamer (0 kJ mol^{-1}), (B) helical foldamer with lone-pair−π interactions (+0.9 kJ mol^{-1}) and (C) unfolded oligomer (+95 kJ mol^{-1}).

oligomers without any contacts between the NDI were much less stable, e.g., +95 kJ mol^{-1} for trimer **3″** (Figure 4C). Helical conformers stabilized by lone-pair−π interactions from one imide oxygen to the aromatic surface occurred at only slightly higher energy, e.g., +0.9 kJ mol^{-1} for trimer **3″**, with O−π distances down to 2.97 Å (Figure 4B). However, results from NMR spectra, DOSY, CV and ratiometric absorption demonstrated that only one conformer is strongly preferred and that the NDIs of this conformer share electrons, which rules out all but face-to-face π-stacked foldamers (Figures 1, 2, 3 and 4A). The underestimation of their stability compared to stack-free, partially unfolded conformers (Figure 4B) in computational models is likely to originate from entropic contributions because largest contact areas in π-stacked foldamers result in highest desolvation. These entropic contributions have been identified as dominant driving force in foldamer chemistry and self-assembly but passed unnoticed

DOI: 10.1021/jacs.8b00809
J. Am. Chem. Soc. 2018, 140, 4884−4892

in calculations that represent solvent as a continuous medium.[24,26]

In the preferred face-to-face π-stacked foldamers, the distances between the first two NDI planes decreased from dimer **2″** with 3.53 Å to 3.46 Å for tetramer **4″** and 3.44 Å for a hypothetical pentamer (Figure S13, Table 1). Consistent with experimental results on electron sharing from absorbance ratio and decreasing LUMO energy, this increasing π stacking with increasing foldamer length was sublinear and showed good agreement with a power fit. Axial views of the foldamers revealed that the twist angle between adjacent NDIs gradually decreased with increasing stack length (Figure S14). The decrease for the peripheral twist from 29.8° in dimer **2″** to minimal 26.9° in hypothetical pentamer **5″** was relatively minor. The smallest twist in the center of the stacks, however, decreased from 29.8° dimer **2″** to 21.2° in tetramer **4″** and 15.0° in hypothetical pentamer **5″**. This decreasing twist with increasing stack length correlated well with increasing electron sharing in optoelectronic studies.

The molecular electrostatic potential (MEP) surface of monomer **1″** showed maximal +100.0 kJ mol^{-1} on the aromatic π surface (Figure S15). This maximal potential increased to +123.5 kJ mol^{-1} in dimer **2″**. From there, a less pronounced increase around ~ +1.5 kJ mol^{-1} per monomer was observed. Overall, the dependence of the maximal potential to oligomer length was again sublinear.

Chloride binding was negligible to NDI monomer **1″** that does not offer support from additional interactions (E_{int} = −0.1 kJ mol^{-1} Figure 5A, Table 1). With increasing length of the π-stacked foldamers, chloride binding to the π surface increased linearly to maximize for tetramer **4″** at E_{int} = −8.3 kJ mol^{-1} and a hypothetical pentamer at E_{int} = −12.1 kJ mol^{-1} (Figures 5A, S16, S17, Table 1). This increase in binding was reflected in a slight shortening of the distance of the chloride to the π surface, from 2.73 Å in monomer **1″** to 2.71 Å in tetramer **4″** (Figures 5, S16).

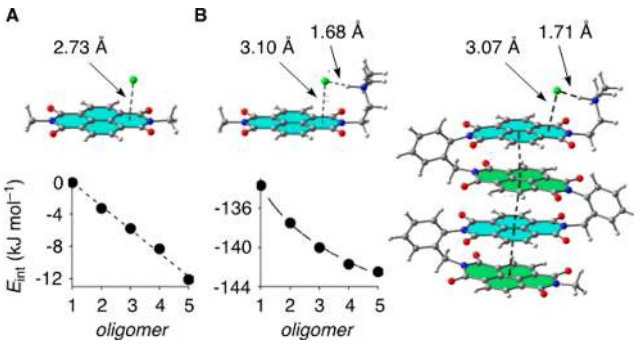

Figure 5. Dependence of interaction energies on foldamer length for chloride binding to **1″**−**4″** and a hypothetical pentamer with terminal methyl groups (A) and to **1′**−**4′** and a hypothetical pentamer with covalent ammonium counterions at one and a Me at the other terminus (B), together with examples for energy-minimized structures of chloride complexes of monomers **1″** and **1′** and tetramer **4′**.

Chloride binding to the (almost) real oligomers **2′**−**4′** with a covalently attached ammonium cation next to the π surface was necessarily dominated by ion pairing. Chloride binding increased with increasing foldamer length by ΔE_{int} = −8.0 kJ mol^{-1} from monomer **1′** to tetramer **4′** (Table 1). This increase was almost identical to the increase computed in the absence of ammonium counterions. The distance of the chloride to the π surface decreased similarly from 3.10 Å in monomer **1′** to 3.07 Å in tetramer **4′**, whereas the hydrogen bond to the counterion increased correspondingly from 1.68 to1.71 Å (Figures 5B, S19).

In the presence of covalent counterions, the contribution per monomer to the chloride binding energy decreased with increasing foldamer length. The resulting overall increase was again sublinear (Figure 5B). This power dependence of chloride binding by foldamers **1′**−**4′** reflected experimental trends on electron sharing from absorption spectra and CV. In clear contrast, the linear increase of chloride binding with increasing length of counterion-free foldamers **1″**−**4″** exceeded expectations from experiments. Overruling the intrinsic sublinear dependence on stack length, these results supported the occurrence of strong synergistic effects between anion−π interactions and π−π interactions within the π stack. The increase of the synergism of chloride−π interactions in the absence of covalent counterions coincided with a shortening of the distance from anion to π surface from 3.10 Å in monomer **1′** to 2.73 Å in **1″** and from 3.07 Å in tetramer **4′** to 2.71 Å in **4″**. This emergence of synergistic effects expressed in the linear dependence of chloride binding to oligomers **1″**−**4″** will be of interest with regard to anion−$(\pi)_n$−π catalysis described in the following.

Anion−$(\pi)_n$−π Catalysis. The addition of malonic acid half thioester (MAHT) **14** to enolate acceptors such as nitroolefin **15** has emerged as the reaction of choice to probe for anion−π catalysis (Figure 6).[3−5] This reaction is at the beginning of all biosynthesis but often disfavored without enzymes.[3−5] Instead of the significant addition product **16**, the irrelevant decarboxylation product **17** is obtained. We have argued early on[3] that this chemoselectivity can be controlled on the level of

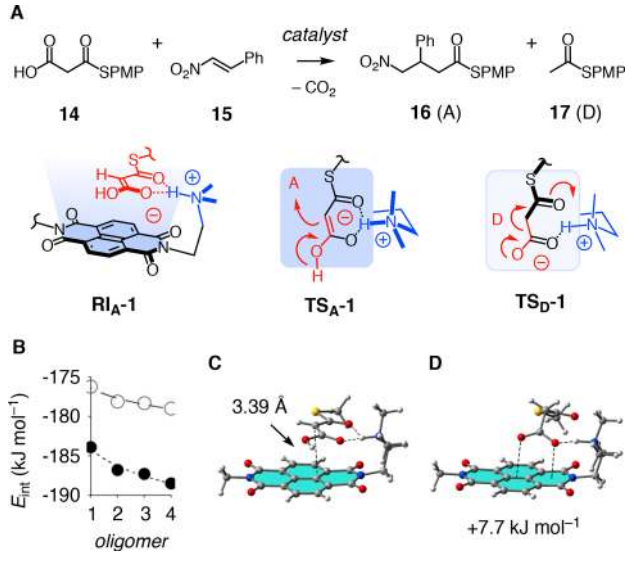

Figure 6. (A) Selective catalysis of the addition of MAHT **14** to acceptor **15** to afford addition product **16** rather than decarboxylation product **17** is envisioned by discrimination between enol tautomers as in reactive intermediate **RI$_A$-1** and transition state **TS$_A$-1** and keto tautomers as in **TS$_D$-1**. (B) Dependence of interaction energies on foldamer length for binding of enol (●) and keto (○) tautomers (as in **TS$_A$-1** and **TS$_D$-1**) to **1′**−**4′**, with examples for energy-minimized structures of enol (C) and keto (D) tautomers bound to monomer **1′** (Me instead of PMP thioester, PMP = *p*-methoxyphenyl, models with PMP gave the same trends, Figure S24).

DOI: 10.1021/jacs.8b00809
J. Am. Chem. Soc. 2018, 140, 4884−4892

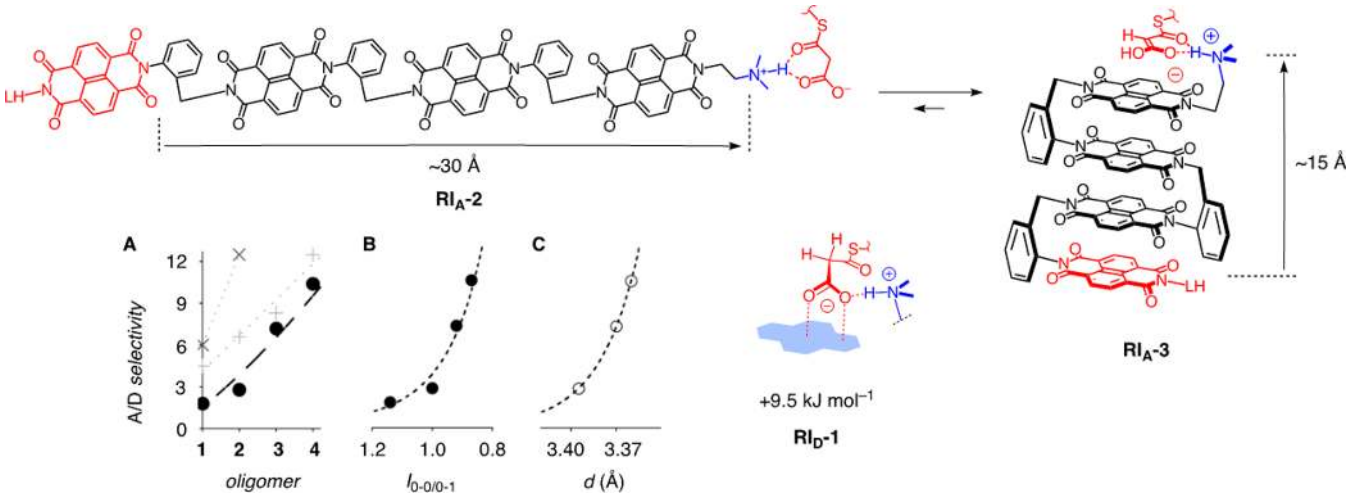

Figure 7. Dependence of the *A*/*D* chemoselectivity of the reaction of MAHT **14** with enolate acceptor **15**, i.e., the yield of addition product **16** divided by the yield of decarboxylation product **17** (Figure 6), on (A) the length of foldamer catalysts **1**−**4** (with linear fit; measured in THF-d_8/$CDCl_3$ 3:1 (●), compared to THF-d_8/$CDCl_3$ 1:1 (+) and analogs with hexyl instead of LH tails in $CDCl_3$ (X), reproducibility was within 3.6% for nine independent experiments), (B) the absorbance ratio, and (C) the computed distance between first and second π plane in the π stack, with power fits and indication of remote control in unfolded and folded reactive intermediates **RI$_A$-2** and **RI$_A$-3** of tetramer **4**.

tautomers of the anionic malonate half thioester (MHT) intermediates obtained by deprotonation of substrate **14**. Namely, "enol" tautomers as in reactive intermediate **RI$_A$-1** and transition state **TS$_A$-1** have to undergo the addition reaction before decarboxylation, whereas "keto" tautomers as in reactive intermediate **TS$_D$-1** can decarboxylate before addition. With an sp^2 α carbon, additive tautomers as in **TS$_A$-1** are planar, and the negative charge is fully delocalized. Decarboxylative tautomers as in **TS$_D$-1** have an sp^3 α carbon, are thus bent and have their negative charge localized on the carboxylate. From the beginning,[3] we have thought that π-acidic surfaces would be perfect to feel the subtle difference between these tautomers, that is planar against bent intermediates with delocalized against localized negative charge. Experimental trends from various systems were consistent with these meaningful speculations and used to support, *inter alia*, existence and significance of anion−π catalysis as such[3,33] as well as the successful creation of anion−π enzymes[34] and electric-field-mediated anion−π catalysis.[4]

Theoretical studies conducted here for the first time proved that these intuitive arguments are correct. In energy-minimized models, the recognition of the planar enol tautomer on monomer **1**′ exceeded that of the bent keto tautomer by ΔE_{int} = −7.7 kJ mol^{-1} (Figure 6C,D, Table 1). The obtained structures feature the planar enol tautomer bound parallel to the π surface at a distance d = 3.39 Å, comparable to that of chloride complexes (Figure 5). In clear contrast, the bent tautomer interacted with the π surface with an edge-to-face carboxylate that carries the full negative charge. For practical reasons, most calculations were done with model intermediates with methyl thioesters (Figure 6B−D, Table 1). Controls with *p*-methoxyphenyl (PMP) thioesters as in substrate **14** on monomers **1**′ gave nearly identical structures with even slightly higher tautomer recognition (ΔE_{int} = −10.0 kJ mol^{-1}, d = 3.37 Å, Figure S24).

As for chloride binding, the binding of both enol and keto tautomers was characterized by a sublinear increase with NDI foldamers length to reach E_{int} = −188.5 kJ mol^{-1} and E_{int} = −179.0 kJ mol^{-1}, respectively, on tetramer **4**′. The empirical apparent power dependence observed previously for the contributions per monomer with increasing stack length applied for both tautomers (Figures 6B, S20−S23). However, the exponent differed significantly. As a result, the selective recognition of the planar enol tautomer over the bent keto tautomer increased with increasing length of the foldamer from E_{int} = −7.7 kJ mol^{-1} on monomer **1**′ to E_{int} = −9.5 kJ mol^{-1} on tetramer **4**′. The resulting ΔE_{int} = −1.8 kJ mol^{-1} promised that contributions from synergistic anion−$(\pi)_n$−π interactions would exist and matter.

The catalytic activity of foldamers **1**−**4** was determined in a mixture of THF-d_8/$CDCl_3$ 3:1 containing 200 mM of MAHT substrate **14** and 2.0 M of enolate acceptor **15** at 20 °C. Under these conditions, control reactions with 20 mol % TEA in place of anion−$(\pi)_n$−π catalysts were very slow and did not reach completion within 2 weeks. With 20 mol % foldamers **1**−**4**, the total conversion was always almost quantitative (>90%).[33] As a measure of chemoselectivity, the yield of the intrinsically disfavored but significant addition (*A*) product **16** was divided by the yield of the decarboxylation (*D*) product. *A*/*D* values <1 thus stand for dominant decarboxylation, *A*/*D* > 1 for dominant addition.

The *A*/*D* = 1.8 obtained with monomer **1** was consistent with similar values obtained previously with similar anion−π catalysts (Table 1).[33] With dimer **2**, selectivity increased to *A*/*D* = 2.8, then further to very significant *A*/*D* = 7.2 and *A*/*D* = 10.4 with trimer **3** and anion−$(\pi)_3$−π catalyst **4**, respectively. The overall most impressive increase from *A*/*D* = 1.8 to *A*/*D* = 10.4 from monomer to tetrameric π stacks provided strong experimental support for existence and relevance of synergistic anion−$(\pi)_n$−π catalysis. "Double-digit" selectivity as for tetramer **4** has so far been achieved only on the large, polarizable π surface of fullerenes.[5]

Moving from THF-d_8/$CDCl_3$ 3:1 to THF-d_8/$CDCl_3$ 1:1, all selectivities increased about the same extent to maximize at *A*/*D* = 13.3 for tetramer **4** (Figure 7A+). This increase should not be overinterpreted because catalysis with the TEA control also becomes faster and with *A*/*D* = 2.1 more selective under these conditions. Even higher selectivities were accessible in $CDCl_3$ with more hydrophobic foldamers having simple hexyl tails in place of the LH tails in the series **1**−**4** (Figure 7AX).

DOI: 10.1021/jacs.8b00809
J. Am. Chem. Soc. 2018, 140, 4884−4892

Although promising A/D = 6.0 and 12.5 were found for monomers and dimers, respectively, trimer catalysts gave an unchanged A/D = 12.7 probably due to their low solubility thus the lower effective concentration in solution. Because solubility problems increase with increasing foldamer length, the hexyl series was discontinued (not shown). Kinetics were consistent with previously reported trends for other systems (Figures S1, S2).[3] Reproducibility of A/D values was within 3.6% for nine independent experiments made in parallel with identical starting materials (catalysts, substrates, solvents, etc.). Systematic errors in the comparison between different batches are more difficult to quantify (e.g., possibly different amounts of absorbed moisture or residual solvents that could affect balancing, water content in solvents), but they were confirmed to be small enough not to influence the overall trends, particularly because the observed differences in activity were so large.

The catalytic activity of monomer **1** (20 mol%) was also measured in the presence of 0, 20, 40, and 60 mol% of dialkyl NDI **11** to mimic the total NDI concentration with dimer **2**, trimer **3** and tetramer **4**, respectively. However, measured in a mixture of THF-d_8/$CDCl_3$ 1:1 under standard conditions, the selectivity remained constant at $A/D \sim 4.0$ despite the increasing NDI concentration. This result excluded the possibility that the increase of A/D selectivity found with increasing foldamer length would be just a consequence of higher absolute concentration of NDI surfaces. Insensitivity of the absorbance ratio $I_{0\text{-}0/0\text{-}1}$ to the presence of substrate **14** supported that the foldamer structure is intact under conditions used for catalysis (Figure S9). Molecular models agreed that there is not enough space also for temporary malonate intercalation into the NDI stacks, and that eventual temporary displacement of NDIs in the stacks by malonate intermediates is unlikely (see above).

The dependence of A/D selectivity on foldamer length was almost linear in both THF-d_8/$CDCl_3$ 3:1 (Figure 7A●) and THF-d_8/$CDCl_3$ 1:1 (Figure 7A+). Largest deviations from linearity were found with **2**, probably because of the poorer π stacking in dimers compared to higher oligomers, as expressed in a longer plane-to-plane distance of d = 3.53 Å (Table 1). The apparent overperformance of dimer **2** in the more hydrophobic environment in THF-d_8/$CDCl_3$ 1:1 could thus be explained with stronger π stacking induced by stronger anion-π interactions with the anionic intermediates and transition states (Figure 7A+). The complementary underperformance of dimer **2** in the less hydrophobic environment in THF-d_8/$CDCl_3$ 3:1 would then originate from less support from anion-π interactions to strengthen the fragile π stacking (Figure 7A●).

The linear dependence of anion$-(\pi)_n-\pi$ catalysis on foldamer length (Figure 7A) was in contrast to the sublinear dependence of absorbance ratio and LUMO energy levels (Figure 2D,E). This suggested that diminishing return on electron sharing with increasing stack length are compensated or even slightly overcompensated by synergistic contributions from anion$-(\pi)_n-\pi$ interactions with anionic intermediates and transition states of the catalyzed reaction. This synergism was best expressed in the dependence of the A/D selectivity on the absorbance ratio of anion$-(\pi)_n-\pi$ catalysts **1**–**4** (Figure 7B). The result of this comparison was pronounced superlinearity.

CONCLUSIONS

The objective of this study was to explore the possible existence and significance of anion$-(\pi)_n-\pi$ catalysis. The idea was that the stabilization of anionic intermediates and transition states by anion$-\pi$ interactions on π-acidic surfaces could be amplified by electron sharing within π stacks. To elaborate on these expectations, a concise series of π-stacked NDI foldamers was designed, synthesized and evaluated. Their optoelectronic properties, that is inversion of absorbance ratio and decreasing LUMO energies, were consistent with increasing electron sharing with increasing stack length. With diminishing returns per monomer with increasing length, they obeyed the sublinear power laws of oligomer chemistry. In computational models, chloride$-\pi$ interactions, enolate$-\pi$ interactions, tautomer discrimination and anion-stack and intrastack distances all responded to increasing stack length, following the same sublinear power dependence.

Experimental results on anion$-(\pi)_n-\pi$ catalysis violated the sublinear power law of oligomer chemistry. The selectivity increased with increasing stack length in a roughly linear manner (Figure 7A). Comparison against the underlying trends from optoelectronic properties and theoretical predictions revealed quite remarkable superlinearity (Figure 7B,C). This superlinearity demonstrated that the identified power of anion$-(\pi)_n-\pi$ catalysis originates from operational synergism between anion$-\pi$ and $\pi-\pi$ interactions, i.e., electron sharing over a very long distance. Moving from trimers to tetramers, the longest oligomers covered in this study, the linear increase in activity at the active site at one terminus caused by the addition of a monomer at the other terminus occurs over a distance of ∼30 Å in unfolded oligomers and still over a distance of ∼15 Å in the preferred foldamers ($\mathbf{RI_A}$-**2**, $\mathbf{RI_A}$-**3**, Figure 7). The synergistic effect can be best imagined with a molecular accordion. Anion$-\pi$ interactions with the reactive intermediates and transition states at one terminus and $\pi-\pi$ interactions with the newly added π surface at the other terminus press the entire stack together to synergistically amplify electron sharing and thus catalysis (Figure 7C).

The music made by these molecular accordions could not sound better: Remote control of synergistic anion$-(\pi)_n-\pi$ catalysis provides access to outstanding activities. This new concept is also most attractive because it identifies unique advantages of anion-π catalysis. Significant cation$-(\pi)_n-\pi$ catalysis is inconceivable because the repulsive π-basic aromatics will not fold into covalent face-to-face π stacks. With regard to perspectives, one big question stands out: Where does it stop?[35] Violating the sublinear power laws of diminishing returns with increasing length, linear increase of activity with length promises access to more and more powerful anion$-(\pi)_n-\pi$ catalysis on longer and longer π stacks. This question is tantalizing because stack elongation beyond the reported tetramers calls for significant synthetic efforts, including strategies to avoid increasing solubility problems. Studies in this direction are ongoing despite these significant challenges, results will be reported in due course.

ASSOCIATED CONTENT

Supporting Information

The Supporting Information is available free of charge on the ACS Publications website at DOI: 10.1021/jacs.8b00809.

Detailed experimental procedures (PDF)

DOI: 10.1021/jacs.8b00809
J. Am. Chem. Soc. 2018, 140, 4884–4892

AUTHOR INFORMATION

Corresponding Author

*stefan.matile@unige.ch

ORCID

Antonio Bauzá: 0000-0002-5793-781X
Antonio Frontera: 0000-0001-7840-2139
Eric Vauthey: 0000-0002-9580-9683
Stefan Matile: 0000-0002-8537-8349

Notes

The authors declare no competing financial interest.

ACKNOWLEDGMENTS

We thank the NMR and the MS platforms for services, and the University of Geneva, the Swiss National Centre of Competence in Research (NCCR) Molecular Systems Engineering, the NCCR Chemical Biology and the Swiss NSF for financial support. A.B. and A.F. thank MINECO of SPAIN for financial support (projects CTQ2014-57393-C2-1-P and CTQ2017-85821-R, FEDER funds).

REFERENCES

(1) (a) Dougherty, D. A. *Acc. Chem. Res.* **2013**, *46*, 885−893. (b) Kennedy, C. R.; Lin, S.; Jacobsen, E. N. *Angew. Chem., Int. Ed.* **2016**, *55*, 12596−12624. (c) Bräuer, T. M.; Zhang, Q.; Tiefenbacher, K. *Angew. Chem., Int. Ed.* **2016**, *55*, 7698−7701. (d) Hart-Cooper, W. M.; Clary, K. N.; Toste, F. D.; Bergman, R. G.; Raymond, K. N. *J. Am. Chem. Soc.* **2012**, *134*, 17873−17876.

(2) (a) Giese, M.; Albrecht, M.; Rissanen, K. *Chem. Commun.* **2016**, *52*, 1778−1795. (b) Chifotides, H. T.; Dunbar, K. R. *Acc. Chem. Res.* **2013**, *46*, 894−906. (c) Wang, D.-X.; Wang, M.-X. *Chimia* **2011**, *65*, 939−943. (d) Ballester, P. *Acc. Chem. Res.* **2013**, *46*, 874−884. (e) He, Q.; Ao, Y.-F.; Huang, Z.-T.; Wang, D.-X. *Angew. Chem., Int. Ed.* **2015**, *54*, 11785−11790. (f) Liao, J.-Z.; Wu, C.; Wu, X.-Y.; Deng, S.-Q.; Lu, C.-Z. *Chem. Commun.* **2016**, *52*, 7394−7397. (g) Liu, J.-J.; Guan, Y.-F.; Jiao, C.; Lin, M.-J.; Huang, C.-C.; Dai, W.-X. *Dalton Trans.* **2015**, *44*, 5957−5960. (h) Kumar, S.; Ajayakumar, M. R.; Hundal, G.; Mukhopadhyay, P. *J. Am. Chem. Soc.* **2014**, *136*, 12004−12010. (i) Bauzà, A.; Mooibroek, T. J.; Frontera, A. *ChemPhysChem* **2015**, *16*, 2496−2517. (j) Yu, Z.; Erbas, A.; Tantakitti, F.; Palmer, L. C.; Jackman, J. A.; Olvera de la Cruz, M.; Cho, M.-J.; Stupp, S. I. *J. Am. Chem. Soc.* **2017**, *139*, 7823−7830. (k) Bélanger-Chabot, G.; Ali, A.; Gabbaï, F. P. *Angew. Chem., Int. Ed.* **2017**, *56*, 9958−9961.

(3) Zhao, Y.; Benz, S.; Sakai, N.; Matile, S. *Chem. Sci.* **2015**, *6*, 6219−6223.

(4) Akamatsu, M.; Sakai, N.; Matile, S. *J. Am. Chem. Soc.* **2017**, *139*, 6558−6561.

(5) (a) López-Andarias, J.; Frontera, A.; Matile, S. *J. Am. Chem. Soc.* **2017**, *139*, 13296−13299. (b) Zhang, X.; Liu, L.; López-Andarias, J.; Wang, C.; Sakai, N.; Matile, S. *Helv. Chim. Acta* **2018**, *101*, e1700288.

(6) (a) Frontera, A.; Quinonero, D.; Garau, C.; Costa, A.; Ballester, P.; Deya, P. M. *J. Phys. Chem. A* **2006**, *110*, 9307−9309. (b) Frontera, A.; Quinonero, D.; Costa, A.; Ballester, P.; Deya, P. M. *New J. Chem.* **2007**, *31*, 556−560.

(7) (a) Al Kobaisi, M.; Bhosale, Si. V.; Latham, K.; Raynor, A. M.; Bhosale, Sh. V. *Chem. Rev.* **2016**, *116*, 11685−11796. (b) Suraru, S.-L.; Würthner, F. *Angew. Chem., Int. Ed.* **2014**, *53*, 7428−7448.

(8) (a) Gorteau, V.; Bollot, G.; Mareda, J.; Perez-Velasco, A.; Matile, S. *J. Am. Chem. Soc.* **2006**, *128*, 14788−14789. (b) Misek, J.; Vargas Jentzsch, A.; Sakurai, S.; Emery, D.; Mareda, J.; Matile, S. *Angew. Chem., Int. Ed.* **2010**, *49*, 7680−7683.

(9) (a) Zhan, X.; Facchetti, A.; Barlow, S.; Marks, T. J.; Ratner, M. A.; Wasielewski, M. R.; Marder, S. R. *Adv. Mater.* **2011**, *23*, 268−284. (b) Sakai, N.; Sisson, A. L.; Bürgi, T.; Matile, S. *J. Am. Chem. Soc.* **2007**, *129*, 15758−15759. (c) Sakai, N.; Matile, S. *J. Am. Chem. Soc.* **2011**, *133*, 18542−18545.

(10) Talukdar, P.; Bollot, G.; Mareda, J.; Sakai, N.; Matile, S. *Chem. - Eur. J.* **2005**, *11*, 6525−6532.

(11) Lee, K. S.; Parquette, J. R. *Chem. Commun.* **2015**, *51*, 15653−15656.

(12) Schneebeli, S. T.; Frasconi, M.; Liu, Z.; Wu, Y.; Gardner, D. M.; Strutt, N. L.; Cheng, C.; Carmieli, R.; Wasielewski, M. R.; Stoddart, J. F. *Angew. Chem., Int. Ed.* **2013**, *52*, 13100−13104.

(13) Shao, H.; Gao, M.; Kim, S. H.; Jaroniec, C. P.; Parquette, J. R. *Chem. - Eur. J.* **2011**, *17*, 12882−12885. (b) Pantoş, G. D.; Wietor, J.-L.; Sanders, J. K. M. *Angew. Chem., Int. Ed.* **2007**, *46*, 2238−2240.

(14) (a) Rajdev, P.; Molla, M. R.; Ghosh, S. *Langmuir* **2014**, *30*, 1969−1976. (b) Mondal, T.; Sakurai, T.; Yoneda, S.; Seki, S.; Ghosh, S. *Macromolecules* **2015**, *48*, 879−888.

(15) Avinash, M. B.; Govindaraju, T. *Adv. Funct. Mater.* **2011**, *21*, 3875−3882.

(16) Goskulwad, S. P.; La, D. D.; Bhosale, R. S.; Al Kobaisi, M.; Bhosale, S. V.; Bhosale, S. V. *RSC Adv.* **2016**, *6*, 39392−39395.

(17) (a) Wu, Y.; Frasconi, M.; Gardner, D. M.; McGonigal, P. R.; Schneebeli, S. T.; Wasielewski, M. R.; Stoddart, J. F. *Angew. Chem., Int. Ed.* **2014**, *53*, 9476−9481. (b) Gabutti, S.; Schaffner, S.; Neuburger, M.; Fischer, M.; Schäfer, G.; Mayor, M. *Org. Biomol. Chem.* **2009**, *7*, 3222−3229. (c) Sao, S.; Samanta, B. R.; Chaudhuri, D. *RSC Adv.* **2016**, *6*, 34350−34353.

(18) Takai, A.; Yasuda, T.; Ishizuka, T.; Kojima, T.; Takeuchi, M. *Angew. Chem., Int. Ed.* **2013**, *52*, 9167−9171.

(19) Gabriel, G. J.; Iverson, B. L. *J. Am. Chem. Soc.* **2002**, *124*, 15174−15175.

(20) Ikkanda, B. A.; Samuel, S. A.; Iverson, B. L. *J. Org. Chem.* **2014**, *79*, 2029−2037.

(21) Miller, L. L.; Duan, R. G.; Tully, D. C.; Tomalia, D. A. *J. Am. Chem. Soc.* **1997**, *119*, 1005−1010.

(22) Avestro, A.-J.; Gardner, D. M.; Vermeulen, N. A.; Wilson, E. A.; Schneebeli, S. T.; Whalley, A. C.; Belowich, M. E.; Carmieli, R.; Wasielewski, M. R.; Stoddart, J. F. *Angew. Chem., Int. Ed.* **2014**, *53*, 4442−4449.

(23) Ashkenasy, N.; Horne, W. S.; Ghadiri, M. R. *Small* **2006**, *2*, 99−102.

(24) (a) Gellman, S. H. *Acc. Chem. Res.* **1998**, *31*, 173−180. (b) Hill, D. J.; Mio, M. J.; Prince, R. B.; Hughes, T. S.; Moore, J. S. *Chem. Rev.* **2001**, *101*, 3893−4012. (c) Schmitt, J.-L.; Stadler, A.-M.; Kyritsakas, N.; Lehn, J.-M. *Helv. Chim. Acta* **2003**, *86*, 1598−1624. (d) Seebach, D.; Beck, A. K.; Bierbaum, D. J. *Chem. Biodiversity* **2004**, *1*, 1111−1239. (e) Guichard, G.; Huc, I. *Chem. Commun.* **2011**, *47*, 5933−5941. (f) Zhang, D. W.; Zhao, X.; Hou, J. L.; Li, Z. T. *Chem. Rev.* **2012**, *112*, 5271−5316. (g) Ando, S.; Ohta, E.; Kosaka, A.; Hashizume, D.; Koshino, H.; Fukushima, T.; Aida, T. *J. Am. Chem. Soc.* **2012**, *134*, 11084−11087. (h) Yashima, E.; Ousaka, N.; Taura, D.; Shimomura, K.; Ikai, T.; Maeda, K. *Chem. Rev.* **2016**, *116*, 13752−13990. (i) Huo, Y.; Zeng, H. *Acc. Chem. Res.* **2016**, *49*, 922−930. (j) Meudtner, R. M.; Hecht, S. *Angew. Chem., Int. Ed.* **2008**, *47*, 4926−4930. (k) Saraogi, I.; Hamilton, A. D. *Chem. Soc. Rev.* **2009**, *38*, 1726−1743. (l) Mendez-Ardoy, A.; Markandeya, N.; Li, X.; Tsai, Y.-T.; Pecastaings, G.; Buffeteau, T.; Maurizot, V.; Muccioli, L.; Castet, F.; Huc, I.; Bassani, D. M. *Chem. Sci.* **2017**, *8*, 7251−7257. (m) Lamouroux, A.; Sebaoun, L.; Wicher, B.; Kauffmann, B.; Ferrand, Y.; Maurizot, V.; Huc, I. *J. Am. Chem. Soc.* **2017**, *139*, 14668−14675.

(25) Jeannerat, D.; Ronan, D.; Baudry, Y.; Pinto, A.; Saulnier, J.-P.; Matile, S. *Helv. Chim. Acta* **2004**, *87*, 2190−2207.

(26) Ikemoto, K.; Kobayashi, R.; Sato, S.; Isobe, H. *Angew. Chem., Int. Ed.* **2017**, *56*, 6511−6514.

(27) Cohen, Y.; Avram, L.; Frish, L. *Angew. Chem., Int. Ed.* **2005**, *44*, 520−554.

(28) Barros, T. C.; Brochsztain, S.; Toscano, V. G.; Filho, P. B.; Politi, M. J. *J. Photochem. Photobiol., A* **1997**, *111*, 97−104.

(29) (a) Spano, F. C. *Acc. Chem. Res.* **2010**, *43*, 429−439. (b) Hestand, N. J.; Spano, F. C. *Acc. Chem. Res.* **2017**, *50*, 341−350.

(30) (a) Wang, J.; Kulago, A.; Browne, W. R.; Feringa, B. L. *J. Am. Chem. Soc.* **2010**, *132*, 4191−4196. (b) Fimmel, B.; Son, M.; Sung, Y. M.; Grüne, M.; Engels, B.; Kim, D.; Würthner, F. *Chem. - Eur. J.* **2015**,

DOI: 10.1021/jacs.8b00809
J. Am. Chem. Soc. 2018, 140, 4884−4892

21, 615−630. (c) Giaimo, J. M.; Lockard, J. V.; Sinks, L. E.; Scott, A. M.; Wilson, T. M.; Wasielewski, M. R. *J. Phys. Chem. A* **2008**, *112*, 2322−2330.
(31) (a) Greenfield, S. R.; Svec, W. A.; Gosztola, D.; Wasielewski, M. R. *J. Am. Chem. Soc.* **1996**, *118*, 6767−6777.
(32) Yushchenko, O.; Licari, G.; Mosquera-Vazquez, S.; Sakai, N.; Matile, S.; Vauthey, E. *J. Phys. Chem. Lett.* **2015**, *6*, 2096−2100.
(33) Cotelle, Y.; Benz, S.; Avestro, A.-J.; Ward, T. R.; Sakai, N.; Matile, S. *Angew. Chem., Int. Ed.* **2016**, *55*, 4275−4279.
(34) Cotelle, Y.; Lebrun, V.; Sakai, N.; Ward, T. R.; Matile, S. *ACS Cent. Sci.* **2016**, *2*, 388−393.
(35) (a) Le Bailly, B. A. F.; Byrne, L.; Clayden, J. *Angew. Chem., Int. Ed.* **2016**, *55*, 2132−2136. (b) Byrne, L.; Solà, J.; Boddaert, T.; Marcelli, T.; Adams, R. W.; Morris, G. A.; Clayden, J. *Angew. Chem., Int. Ed.* **2014**, *53*, 151−155. (c) Diemer, V.; Fischer, L.; Kauffmann, B.; Guichard, G. *Chem. - Eur. J.* **2016**, *22*, 15684−15692.

DOI: 10.1021/jacs.8b00809
J. Am. Chem. Soc. 2018, 140, 4884−4892